Mechanics of Advanced Composite Structures 5 (2018) 49–66

Mechanics of Advanced Composite Structures

Journal homepage: http://MACS.journals.semnan.ac.ir

Semnan University

Three-dimensional elasticity solution for vibrational analysis of thick continuously graded sandwich plates with different boundary conditions using a two-parameter micromechanical model for agglomeration

V. Tahouneh*

*Department of Mechanical Engineering, Islamshahr Branch, Islamic Azad University, Tehran, Iran.

PAPER INFO

Paper history:
Received 2017-06-04
Revised 2017-08-25
Accepted 2017-09-27

Keywords:
Mori-Tanaka approach
Two-parameter model of agglomeration
Sandwich structures
2D generalized differential quadrature method
Vibration analysis

ABSTRACT

An equivalent continuum model based on the Eshelby-Mori-Tanaka approach was employed to estimate the effective constitutive law for an elastic isotropic medium (i.e., the matrix) with oriented straight carbon nanotubes (CNTs). The two-dimensional generalized differential quadrature method was an efficient and accurate numerical tool for discretizing equations of motion and for implementing various boundary conditions. The proposed rectangular plates have two opposite edges simply supported, and all possible combinations of free, simply supported, and clamped boundary conditions were applied to the other two edges. The CNTs volume fraction varied based on the thickness of the functionally graded carbon nanotube-reinforced plate and the generalized power-law distribution of four parameters. The effects of geometrical and material parameters and boundary conditions on the frequency parameters of the laminated functionally graded nanocomposite plates were investigated, and the results revealed that the natural frequencies of the structure were significantly affected by the influence of CNT agglomeration.

1. Introduction

Functionally graded materials (FGMs) are advanced composite materials engineered for smooth spatial variation among material properties, which is achieved by fabricating composite materials with gradual spatial variations among constituent materials' relative volume fractions and microstructures [1].

Malekzadeh, Golbahar, Haghighi, and Atashi [2] performed a free vibration analysis of functionally graded, thin to moderately thick annular plates subjected to a thermal environment and supported on a two-parameter elastic foundation based on the first-order shear deformation theory and differential quadrature method (DQM). Hosseini-Hashemi, Es'haghi, and Karimi [3] performed a vibration analysis of piezoelectric-coupled thick annular functionally graded plates subjected to different combinations of boundary conditions at the inner and outer edges of an annular plate, based on Reddy's third-order shear deformation theory. Free and forced vibrations of functionally graded annular sectorial plates with simply supported radial edges and arbitrary circular edges were investigated by Nie and Zhong [4]. Yas and Tahouneh [5] performed a free vibration analysis of thick functionally graded annular plates on elastic foundations using the DQM and the three-dimensional (3-D) elasticity theory. The same authors [6–9] investigated free vibrations among thick one- and two-directional (2-D) functionally graded

* Corresponding author. Tel.: +98-912-2878681
E-mail address: vahid.tahouneh@ut.ac.ir

DOI: 10.22075/MACS.2018.11539.1111

annular sector plates on Pasternak elastic foundations using the DQM. Tahouneh et al. [10] studied free vibration characteristics of annular continuous-grading fiber reinforced plates resting on elastic foundations using the DQM. Arefi [11] proposed an elastic solution for a curved beam made of FGMs with different cross sections. Bennai, Atmane, and Tounsi [12] developed a new refined hyperbolic shear and normal deformation beam theory to study the free vibrations and buckling of functionally graded sandwich beams under various boundary conditions. Tahouneh [13] used a semi-analytical approach based on the DQM and a series solution to present a 3-D elasticity solution for free vibration analysis of thick continuously graded carbon nanotube-reinforced rectangular plates. Yas and Sobhani Aragh [14] achieved natural frequencies for rectangular continuously graded fiber reinforced plates resting on elastic foundations. Matsunaga [15] analyzed the natural frequencies and buckling stresses of functionally graded plates using a higher order shear deformation theory based on the through thickness series expansion of displacement components. Hosseini-Hashemi, Rokni Damavandi Taher, and Akhavan [16] employed the DQM to investigate free vibrations of functionally graded circular and annular sectorial thin plates of variable thicknesses resting on the Pasternak elastic foundation.

Carbon nanotubes (CNTs) possess exceptional electrical, mechanical, and thermal properties that are relevant for various applications ranging from nano-electronics to biomedical devices. A detailed summary of the mechanical properties of CNTs can be found in [17]. The addition of nano-sized fibers or nanofillers, such as CNTs, can further increase the merits of polymer composites [18]. These nanocomposites, easily processed due to the small diameter of the CNTs, exhibit unique properties [19–20], such as enhanced modulus and tensile strength, high thermal stability, and environmental resistance. This behavior, combined with low density makes CNTs suitable for a broad range of technological sectors, including telecommunication, electronic [21], and transport industries, and particularly for aeronautic and aerospace applications for which reduced weight is crucial to reducing fuel consumption. For example, Qian et al. [22] showed that the addition of a 1 wt. % (i.e., 1% by weight) multiwall CNT to polystyrene resulted in 36–42% and 25% increases in the elastic modulus and the break stress of the nanocomposite properties, respectively. In addition, Yokozeki, Iwahori, and Ishiwata [23] reported the retardation of the onset of matrix cracking in composite laminates containing cup-stacked CNTs compared to those without such CNTs. The properties of the CNT-reinforced composites (CNTRCs) depend on a variety of parameters, including CNT geometry and the interphase between the matrix and CNT. Interfacial bonding in the interphase region between an embedded CNT and its surrounding polymer is a crucial issue for load transferring and reinforcement [24]. Experimental and numerical studies of CNTRCs have shown that distributing CNTs uniformly for reinforcement in a matrix can achieve moderate improvements of mechanical properties [22, 25] due to the weak interface between the CNTs and the matrix where a significant material property mismatch exists.

FGMs can be utilized to manage a material's microstructure and to improve the vibrational behavior of a plate or shell structure reinforced by CNTs. In the literature, few studies on the mechanical behavior of functionally graded CNTRC structures have been performed. Shen [26] suggested that nonlinear bending behavior can be considerably improved through the use of a functionally graded distribution of CNTs in a matrix. The compressive post-buckling and thermal buckling behaviors of functionally graded nanocomposite plates reinforced by aligned, straight single-wall CNTs (SWCNTs) subjected to in-plane temperature variation were reported by Shen and Zhu [27] and Shen and Zhang [28]. Ke, Yang, and Kitipornchai [29] investigated the nonlinear free vibration of functionally graded CNTRC Timoshenko beams and found that both linear and nonlinear frequencies of functionally graded CNTRC beam with symmetrical distribution of CNTs were higher than those of beams with uniform or unsymmetrical distribution of CNTs. Marin and Lupu [30] obtained a spatial estimate, similar to the Saint-Venant type using Toupin-type measure associated with corresponding steady-state vibrations and assumed that the exciting frequency was lower to a certain critical frequency. Marin [31] extended the concept of domain of influence to cover the elasticity of microstretch materials. Sharma and Marin [32] studied wave propagation in micropolar thermoelastic solid half space with distinct conductive and thermodynamic temperatures by examining the oblique reflection of a plane waves incident at the free surface of the micropolar generalized thermoelastic solid half space at two temperatures.

Although research has been conducted on general sandwich structures, very little work has been done to consider the vibrational behavior of functionally graded sandwich structures [33,34]. Li, Iu, and Kou [35] studied free vibrations of functionally graded sandwich rectangular plates with simply supported and clamped edges. Kamarian, Yas, and Pourasghar [36] studied free vibration of functionally graded sandwich rectangular plates with simply supported edges, resting on elastic foundations using the DQM. Very recently, Wand and Shen [37] investigated the large amplitude vibration and the nonlinear bending of a sandwich plate with CNTRC face sheets resting on an elastic foundation based on a micromechanical

model and multi-scale approach. Tahouneh and Naei [38] investigated free vibration and vibrational displacements of thick laminated curved panels with finite using the DQM. It was assumed that the inner surfaces of the functionally graded sheets were metal rich, while the outer surface layers were metal or ceramic rich or made of a mixture of two constituents. Moradi-Dastjerdi [39] investigated the effect of wave propagation in functionally graded composite cylinders reinforced by aggregated CNTs. Moradi-Dastjerdi and Momeni-Khabisi [40] studied free and forced vibrations and resonance phenomena in sandwich plates with an isotropic core and composite reinforced by wavy CNT face sheets. Moradi-Dastjerdi and Momeni-Khabisi [41] investigated free-vibration and stress-wave propagation behavior in nanocomposite plates reinforced by wavy CNTs using the mesh-free method based on the first order shear deformation theory. Moradi-Dastjerdi and Malek-Mohammadi [42] investigated biaxial buckling of sandwich plates with symmetric composite laminated core and functionally graded face sheets using a new and improved high-order theory. Other research considered vibration and static analyses of functionally graded CNT-reinforced nanocomposite structures [43-45], such as Bouchafa et al. [46], who investigated thermal stress and deflections of functionally graded sandwich plates via a new refined hyperbolic shear deformation theory.

In most of the studies mentioned above, the material properties of functionally graded CNTRCs were assumed to be graded by thickness, which was estimated based on the extended rule of mixtures. Using this rule, CNT efficiency parameters were determined by matching the elastic modulus of CNTRCs from the molecular dynamics (MD) simulation results with numerical results obtained from the extended rule of mixture. The extended rule of mixture is not applicable when CNTs are oriented randomly in the matrix.

CNTs have low bending stiffness, due to a small diameter and small elastic modulus in the radial direction, and a high aspect ratio, allowing for simple agglomeration in polymer matrices [47–48]. To achieve the desired properties for CNTRCs, it is critical to ensure that CNTs are uniformly dispersed in a matrix [49]. It has been observed that a large amount of the nanotubes concentrate in agglomerates [50]; Stephan et al. [51] observed that in a 7.5% concentration sample, a large amount of CNTs were concentrated in aggregates. Other researchers have considered the agglomeration effect of single-walled CNTs on different structures [52–56], such as Tornabene, Fantuzzi, and Bacciocchi [57] who studied the static response of composite plates and shells reinforced by agglomerated nanoparticles made of CNTs. Fantuzzi et al. [58] investigated the free vibration of arbitrary shaped functionally graded CNT-reinforced plates using the non-uniform rational b-spline curve method, which describes arbitrary shapes with holes and discontinuities. The buckling behavior of moderately thick CNT-reinforced spherical composite panels subjected to both uniaxial and biaxial loads was examined by Pouresmaeeli, Fazelzadeh, and Ghavanloo [59], while Tahouneh and Eskandari-Jam [60] performed a free vibration analysis of elastically supported continuously graded CNT-reinforced annular plates. The volume fractions of oriented, straight SWCNTs were assumed to be graded by thickness.

The specific objective of the present investigation is to provide a 3-D elasticity solution for the analysis of the natural frequencies of functionally graded nanocomposite sandwich plates. The volume fractions of randomly oriented agglomerated SWCNTs are assumed to be graded by the thickness of sheets. The direct application of CNT properties in micromechanics models for predicting material properties of nanotube/polymer composites is inappropriate without taking into account the effects of significant size differences between nanotubes and a typical carbon fiber [61]. In other words, continuum micromechanics equations cannot capture the scale difference between the nano and micro levels. To overcome this limitation, a virtual equivalent fiber consisting of a nanotube and its interphase, which is perfectly bonded to surrounding resin, was applied. A two-parameter micromechanics model of agglomeration was used to determine the effect of CNT agglomeration on the elastic properties of randomly oriented CNTRCs. In this research, an equivalent continuum model based on the Eshelby-Mori-Tanaka approach was employed to estimate the effective constitutive law of the elastic isotropic medium (i.e., matrix) with oriented straight CNTs. The generalized DQM was used to solve the governing equations for the sandwich plates.

2. Material properties of CNTRCs

2.1 Properties of the equivalent fiber

A virtual equivalent fiber consisting of a nanotube and its interphase, perfectly bonded to surrounding resin, was used to obtain the mechanical properties of a CNT/polymer composite using the multiscale finite element method (FEM). The equivalent fiber for a SWCNT with a chiral index of (10, 10) was a solid cylinder with diameter of 1.424 nm. The ROM was used inversely to calculate the material properties of the equivalent fiber as follows [62].

$$E_{LEF} = \frac{E_{LC}}{V_{EF}} - \frac{E_M V_M}{V_{EF}}$$
$$\frac{1}{E_{TEF}} = \frac{1}{E_{TC} V_{EF}} - \frac{V_M}{E_M V_{EF}}$$
$$\frac{1}{G_{EF}} = \frac{1}{G_C V_{EF}} - \frac{V_M}{G_M V_{EF}} \quad (1)$$
$$\upsilon_{EF} = \frac{\upsilon_C}{V_{EF}} - \frac{\upsilon_M V_M}{V_{EF}}$$

where E_{LEF}, E_{TEF}, G_{EF}, υ_{EF}, E_{LC}, E_{TC}, G_C, υ_C, E_M, G_M, υ_M, V_{EF}, and V_M were the longitudinal modulus of equivalent fiber, transverse modulus of equivalent fiber, shear modulus of equivalent fiber, Poisson's ratio of equivalent fiber, longitudinal modulus of composites, transverse modulus of composites, shear modulus of composites, Poisson's ratio of composites, modulus of matrix, shear modulus of matrix, Poisson's ratio of matrix, volume fraction of the equivalent fiber, and volume fraction of the matrix, respectively. E_{LC}, G_C, and E_{TC} were obtained using a multiscale FEM or MD simulations, respectively. Mechanical properties of the developed equivalent fiber are listed in Table 1 [24]. In [24], material properties of the matrix were given as $E^m = 2.1GPa, \rho^m = 1150kg/m^3$ and $\upsilon^m = 0.34$.

2.2 Effect of CNT agglomeration on the properties of composites

In CNTRCs and due to large aspect ratios (usually > 1,000), low bending rigidity of CNTs, and van der Waals forces, CNTs have a tendency to bundle or cluster together. The effect of nanotube agglomeration on the elastic properties of randomly oriented CNTRCs is presented in this section. Shi et al. [49] derived a two-parameter micromechanics model to determine the effect of nanotube agglomeration on the elastic properties of randomly oriented CNTRCs (Figure 1). It is assumed that a number of CNTs are uniformly distributed (UD) throughout the matrix and that other CNTs appear in cluster form because of agglomeration, as shown in Figure 1. The total volume of the CNTs in the representative volume element (RVE), denoted by V_r, can be divided into the following two parts:

Table 1. Material properties of the equivalent fiber

Mechanical Properties	Equivalent fiber [62]
Longitudinal Young's Modulus (GPa)	649.12
Transverse Young's Modulus (GPa)	11.27
Longitudinal Shear Modulus (GPa)	5.13
Poisson's Ratio	0.284
Density (kg/m^3)	1400

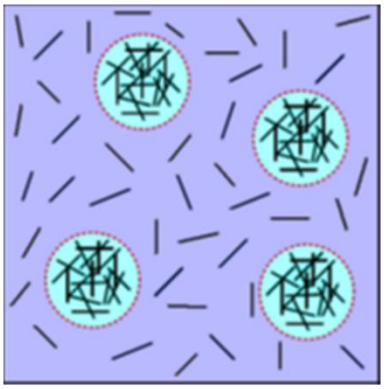

Figure 1. RVE with the Eshelby inclusion model of agglomeration of CNTs

$$V_r = V_r^{cluster} + V_r^m \quad (2)$$

where $V_r^{cluster}$ represents the volumes of CNTs inside a cluster, and V_r^m is the volume of CNTs in the matrix and outside the clusters. The two parameters used to describe the agglomeration are defined as

$$\mu = \frac{V_{cluster}}{V}, \quad \eta = \frac{V_r^{cluster}}{V_r}, \quad \eta \geq 0, \mu \leq 1 \quad (3)$$

where V is the volume of RVE, $V_{cluster}$ is the volume of clusters in the RVE, μ is the volume fraction of clusters with respect to the total volume of the RVE, and η is the volume ratio of the CNTs inside the clusters over the total volume of CNTs inside the RVE. $\mu = 1$ denotes that all CNTs are uniformly dispersed in the matrix, and with the decrease of μ, the agglomeration degree of CNTs is more severe. If $\eta = 1$, all the nanotubes are located in the clusters, while $\mu = \eta$ means that the volume fraction of CNTs inside the clusters is the same as that of CNTs outside the clusters (i.e., CNTs are fully dispersed). When $\mu < \eta$, the larger value of η denotes increased heterogeneous the spatial distribution of CNTs. Thus, CNTRCs, as a system, consist of clusters of sphere shapes embedded in a matrix.

Effective elastic stiffness of the clusters and the matrix should first be estimated before calculating the overall properties of the whole composite system. The effective bulk modulus K_{in} and shear modulus G_{in} of the cluster and the effective bulk modulus K_{out} and shear modulus G_{out} of the equivalent matrix outside the cluster can be calculated by [49]:

$$K_{in} = K_m + \frac{f_r \eta (\delta_r - 3K_m \alpha_r)}{3(\mu - f_r \eta + f_r \eta \alpha_r)}, \quad (4)$$

$$K_{out} = K_m + \frac{f_r (1-\eta)(\delta_r - 3K_m \alpha_r)}{3(1-\mu - f_r (1-\eta) + f_r (1-\eta)\alpha_r)}, \quad (5)$$

$$G_{in} = G_m + \frac{f_r \eta (\eta_r - 2G_m \beta_r)}{2(\mu - f_r \eta + f_r \eta \alpha_r)}, \quad (6)$$

$$G_{out} = G_m + \frac{f_r(1-\eta)(\eta_r - 2G_m\beta_r)}{2(1-\mu - f_r(1-\eta) + f_r(1-\eta)\beta_r)} \quad (7)$$

where

$$\alpha_r = \frac{3(K_m + G_m) + k_r - l_r}{3(G_m + k_r)}, \quad (8)$$

$$\beta_r = \frac{1}{5}\left[\begin{array}{c} \frac{4G_m + 2k_r + l_r}{3(G_m + k_r)} + \frac{4G_m}{G_m + P_r} + \\ \frac{2\left[G_m(3K_m + G_m) + G_m(3K_m + 7G_m)\right]}{G_m(3K_m + G_m) + m_r(3K_m + 7G_m)} \end{array}\right], \quad (9)$$

$$\delta_r = \frac{1}{3}\left[\frac{(2k_r + l_r)(3K_m + 2G_m - l_r)}{G_m + k_r} + n_r + 2l_r\right] \quad (10)$$

$$\eta_r = \frac{1}{5}\left[\begin{array}{c} \frac{2}{3}(n_r - l_r) + \frac{8G_m P_r}{G_m + P_r} + \\ \frac{2(k_r - l_r)(2G_m + l_r)}{3(G_m + k_r)} + \\ \frac{8m_r G_m(3K_m + 4G_m)}{3K_m(m_r + G_m) + G_m(7m_r + G_m)} \end{array}\right] \quad (11)$$

The subscripts m and r stand for the quantities of the matrix and the reinforcing phase; K_m and G_m are the bulk and shear moduli of the matrix, respectively; and k_r, l_r, m_r, n_r, and p_r are the Hill's elastic moduli for the reinforcing phase (i.e., the CNTs), which can be found from the equality of the two following matrices.

$$C_r = \begin{bmatrix} n_r & l_r & l_r & 0 & 0 & 0 \\ l_r & k_r + m_r & k_r - m & 0 & 0 & 0 \\ l_r & k_r - m_r & k_r + m_r & 0 & 0 & 0 \\ 0 & 0 & 0 & p_r & 0 & 0 \\ 0 & 0 & 0 & 0 & m_r & 0 \\ 0 & 0 & 0 & 0 & 0 & p_r \end{bmatrix} \quad (12)$$

$$C_r = \begin{bmatrix} \frac{1}{E_L} & -\frac{\upsilon_{TL}}{E_T} & -\frac{\upsilon_{ZL}}{E_Z} & 0 & 0 & 0 \\ -\frac{\upsilon_{LT}}{E_L} & \frac{1}{E_T} & -\frac{\upsilon_{ZT}}{E_Z} & 0 & 0 & 0 \\ -\frac{\upsilon_{LZ}}{E_L} & -\frac{\upsilon_{TZ}}{E_T} & \frac{1}{E_Z} & 0 & 0 & 0 \\ 0 & 0 & 0 & \frac{1}{G_{TZ}} & 0 & 0 \\ 0 & 0 & 0 & 0 & \frac{1}{G_{ZL}} & 0 \\ 0 & 0 & 0 & 0 & 0 & \frac{1}{G_{LT}} \end{bmatrix}^{-1} \quad (13)$$

Here, E_L, E_T, E_Z, G_{TZ}, G_{ZL}, G_{LT}, and υ_{LT} are material properties of the equivalent fiber, which can be determined from the inverse of the ROM. Before the use of the ROM, material properties of nanoscale RVEs of nanocomposites must be obtained from multiscale FEM analysis or MD simulations. The effective bulk modulus K and the effective shear modulus G of the composite are derived using the MT method as follows [49]:

$$K = K_{out}\left(1 + \frac{\mu(\frac{K_{in}}{K_{out}} - 1)}{1 + \alpha(1-\mu)(\frac{K_{in}}{K_{out}} - 1)}\right), \quad (14)$$

$$G = G_{out}\left(1 + \frac{\mu(\frac{G_{in}}{G_{out}} - 1)}{1 + \beta(1-\mu)(\frac{G_{in}}{G_{out}} - 1)}\right), \quad (15)$$

in which

$$\alpha = \frac{1 + S_{out}}{3(1 - S_{out})}, \quad (16)$$

$$\beta = \frac{2(4 - 5S_{out})}{15(1 - S_{out})}, \quad (17)$$

$$S_{out} = \frac{3K_{out} - 2G_{out}}{2(3K_{out} + G_{0ut})}, \quad (18)$$

Finally, the effective Young's modulus E and Poisson's ratio υ of the composite are given as

$$E = \frac{9KG}{3K + G} \quad (19)$$

$$\upsilon = \frac{3K - 2G}{6K + 2G} \quad (20)$$

3. Problem description

Consider a sandwich rectangular plate with length a, width b, and thickness h as depicted in Figure 2. The deformations defined with reference to a Cartesian coordinate system (x, y, z) are u, v, and w in the x, y, and z directions, respectively. In the present work, V_{cnt} and V_m are the CNT and matrix volume fraction, respectively. It is assumed that the CNT volume fraction varies according to the thickness of the functionally graded carbon nanotube-reinforced(FG-CNTR) plate based on generalized power-law distribution with four parameters [63].

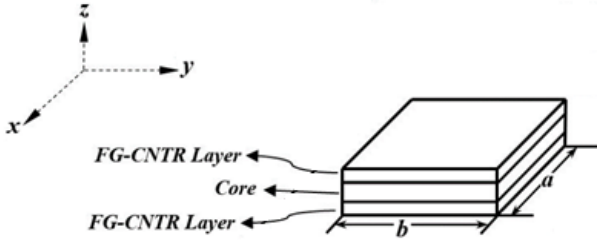

Figure 2. Geometry of a FG-CNTR sandwich plate (the origin is placed in the middle of the sandwich plate)

$$V_{cnt}=\begin{cases}V^{*}(1-(1-a(1-\dfrac{z+0.5}{h_f})+\\ b(1-\dfrac{z+0.5}{h_f})^{c})^{p}) \\ -0.5h\le z\le -0.5h+h_f\end{cases},\quad \begin{cases}0\\ -0.5h+h_f\le z\le 0.5h-h_f\end{cases},\quad \begin{cases}V^{*}(1-(1-a(1+\dfrac{z-0.5}{h_f})+\\ b(1+\dfrac{z-0.5}{h_f})^{c})^{p}) \\ 0.5h-h_f\le z\le 0.5h\end{cases} \tag{21}$$

Here, h and h_f are the thicknesses of the plate and the face sheets, respectively, and V^* is the maximum possible amount of the CNT volume fraction in the face sheets. The volume fraction index p $(0\le p\le\infty)$ and the parameters a, b, and c indicate the CNT volume fraction profile through the thickness of the structure. The values of parameters a, b, and c must be chosen so that $(0\le V_{cnt}\le V^{*})$. According to the relation (21), the core of the structure does not contain CNTs, whereas the lower and upper face sheets are made of a mixture of the two constituents. Various material profiles through the thickness of the face sheets can be illustrated using the four-parameter power-law distribution. The through-thickness variations in the volume fraction for some profiles are illustrated in Figure 3 for different amounts of parameters b, c, and p.

The total volume fractions of CNTs (V_{cnt}^{total}) based on thickness for different types of material distribution profiles (Figures 3A, 3B, and 3C) are reported in Tables 2, 3, and 4.

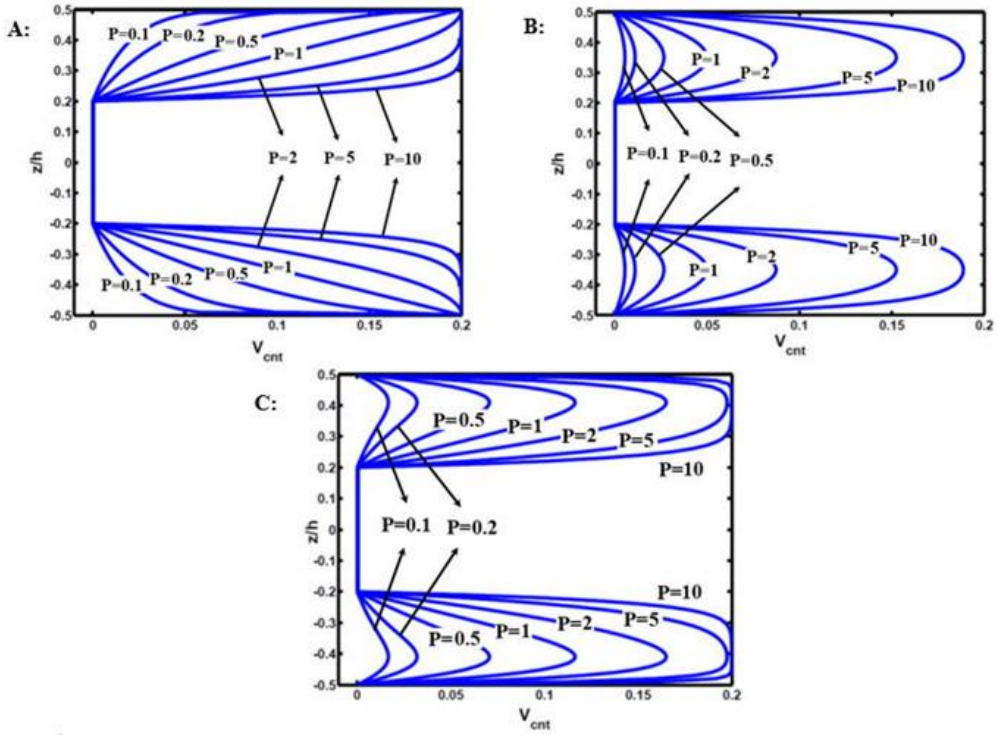

Figure 3. Variation in the fiber volume fraction (Vcnt) through the thickness of the functionally graded sandwich plate. A: (a=1, b=0, c=2), B: (a=1, b=1, c=2), C: (a=1, b=1, c=6)

Table 2. The total volume percentage of CNTs (V_{cnt}^{total}) based on plate thickness with different amounts for parameter "P" for a = 1, b = 0, and c = 2

P=0.1	P=0.2	P=0.5	P=1	P=2	P=5	P=10
1.09	2.00	4.00	6.00	8.00	10.00	10.90

Table 3. The total volume percentage of CNTs (V_{cnt}^{total}) based on plate thickness with different amounts for parameter "P" for a = 1, b = 1, and c = 2

P=0.1	P=0.2	P=0.5	P=1	P=2	P=5	P=10
0.22	0.44	1.05	2.00	3.60	6.76	9.19

Table 4. The total volume fraction of CNTs (V_{cnt}^{total}) based on plate thickness for different amounts of parameter "P" for a = 1, b = 1, and c = 6

P=0.1	P=0.2	P=0.5	P=1	P=2	P=5	P=10
0.56	1.08	2.47	4.28	6.65	9.45	10.66

4. Governing equations and solution procedure

The mechanical constitutive relations that relate stress to strains are as follows [64].

$$\sigma_{ij} = \lambda \varepsilon_{kk} \delta_{ij} + 2\psi \varepsilon_{ij} \tag{22}$$

Here, λ and ψ are the Lame constants, ε_{ij} is the infinitesimal strain tensor, and δ_{ij} is the Kronecker delta. In the absence of body forces, the equations of motion are as follows [64].

$$\begin{aligned} &\frac{\partial \sigma_x}{\partial x} + \frac{\partial \tau_{xy}}{\partial y} + \frac{\partial \tau_{xz}}{\partial z} = \rho \frac{\partial^2 u}{\partial t^2}, \\ &\frac{\partial \tau_{xy}}{\partial x} + \frac{\partial \sigma_y}{\partial y} + \frac{\partial \tau_{yz}}{\partial z} = \rho \frac{\partial^2 v}{\partial t^2}, \\ &\frac{\partial \tau_{xz}}{\partial x} + \frac{\partial \tau_{yz}}{\partial y} + \frac{\partial \sigma_z}{\partial z} = \rho \frac{\partial^2 w}{\partial t^2} \end{aligned} \tag{23}$$

The infinitesimal strain tensor is related to displacement as follows [64],

$$\begin{aligned} &\varepsilon_x = \frac{\partial u}{\partial x}, \varepsilon_y = \frac{\partial v}{\partial y}, \varepsilon_z = \frac{\partial w}{\partial z}, \gamma_{xy} = \frac{\partial u}{\partial y} + \frac{\partial v}{\partial x}, \\ &\gamma_{xz} = \frac{\partial u}{\partial z} + \frac{\partial w}{\partial x}, \gamma_{yz} = \frac{\partial v}{\partial z} + \frac{\partial w}{\partial y} \end{aligned} \tag{24}$$

where u, v, and w are displacement components along the *x*, *y*, and *z* axes, respectively. Upon substituting (24) into (22) and then into (23), the equations of motion in terms of displacement components with infinitesimal deformations can be written as given below.

$$\begin{bmatrix} F_{1x} & F_{1y} & F_{1z} \\ F_{2x} & F_{2y} & F_{2z} \\ F_{3x} & F_{3y} & F_{3z} \end{bmatrix} \begin{Bmatrix} u \\ v \\ w \end{Bmatrix} = \begin{Bmatrix} \rho \frac{\partial^2 u}{\partial t^2} \\ \rho \frac{\partial^2 v}{\partial t^2} \\ \rho \frac{\partial^2 w}{\partial t^2} \end{Bmatrix} \tag{25}$$

The related boundary conditions at *z=-h/2* and *h/2* are as follows:

at *z = -h/2*:

$$\sigma_{zx} = 0, \sigma_{zy} = 0, \sigma_{zz} = 0 \tag{26}$$

and at *z = h/2*:

$$\sigma_{zx} = 0, \sigma_{zy} = 0, \sigma_{zz} = 0 \tag{27}$$

where σ_{ij} are the components of the stress tensor. The stress components are related to the displacement components using 3D constitutive relations as Eq. (28).

$$\begin{aligned} &\sigma_x = c_{11} \frac{\partial u}{\partial x} + c_{12} \frac{\partial v}{\partial y} + c_{13} \frac{\partial w}{\partial z}, \\ &\sigma_{yz} = c_{44} \left(\frac{\partial w}{\partial y} + \frac{\partial v}{\partial z} \right) \\ &\sigma_y = c_{12} \frac{\partial u}{\partial x} + c_{22} \frac{\partial v}{\partial y} + c_{23} \frac{\partial w}{\partial z}, \\ &\sigma_{xz} = c_{55} \left(\frac{\partial u}{\partial z} + \frac{\partial w}{\partial x} \right) \\ &\sigma_z = c_{13} \frac{\partial u}{\partial x} + c_{23} \frac{\partial v}{\partial y} + c_{33} \frac{\partial w}{\partial z}, \\ &\sigma_{xy} = c_{66} \left(\frac{\partial v}{\partial x} + \frac{\partial u}{\partial y} \right) \end{aligned} \tag{28}$$

Different types of classical boundary conditions at the edges of the plate can be stated as follows.

Simply supported (S):

$$\sigma_{yy} = 0, w = 0, u = 0; \tag{29}$$

Clamped (C):

$$u = 0, v = 0, w = 0; \tag{30}$$

Free (F):

$$\sigma_{yy} = 0, \sigma_{xy} = 0, \sigma_{yz} = 0 \tag{31}$$

Here, plates with two opposite edges at *x = -a/2* and *a/2* are simply supported, and arbitrary conditions at edges *y = -b/2* and *b/2* are considered. For free vibration analysis, adopting the following form for the displacement components allows the boundary conditions at edges x = *-a/2* and *a/2* to be satisfied.

$$\begin{aligned} &u(x, y, z, t) = U_m(y, z, t) \cos(m\pi(x + a/2)/a) e^{i\omega t}, \\ &v(x, y, z, t) = V_m(y, z, t) \sin(m\pi(x + a/2)/a) e^{i\omega t}, \\ &w(x, y, z, t) = W_m(y, z, t) \sin(m\pi(x + a/2)/a) e^{i\omega t} \end{aligned} \tag{32}$$

Here, *m* is the wave number along the x-direction, ω is the natural frequency, and i (= $\sqrt{-1}$) is the imaginary number. Substituting displacement components from (32) into the equations of motion for displacement components, the coupled partial differential equations are reduced to a set of coupled ordinary differential equations. The geometric and natural boundary can also be simplified; however, for brevity, this is not shown here.

It is necessary to develop appropriate methods to investigate the mechanical responses of functionally graded nanocomposite sandwich plates. Due to the complexity of the problem caused by inhomogeneity, it is difficult to obtain an exact solution. In this paper, the generalized DQM was used to solve the governing equations of rectangular plates.

Substituting displacement components from (32) in (25), allows for the use of the generalized DQM to discretize the equations of motion. The main difference between this method and others is how governing equations are discretized. In the DQM, governing equations and boundary conditions are directly dis-

cretized; thus, elements of stiffness and mass matrices are evaluated directly. In contrast, in the Rayleigh-Ritz method and FEM, the weak form of the governing equations should be developed and the boundary conditions satisfied in the weak form. By doing this, larger numbers of integrals with increasing amounts of differentiation should be obtained to arrive at the element matrices. Also, the number of degrees of freedom must increase to obtain acceptable accuracy. A brief review of this is given in Shu [65] and Shu and Richards [66]), and the following equations can be given in the *x*-direction:

$$\begin{aligned}
&-(c_{11})_{jk}(\frac{m\pi}{a})^2 U_{mjk} + (c_{12})_{jk}(\frac{m\pi}{a}) \\
&\sum_{n=1}^{N_y} A_{jn}^{y} V_{mnk} + (c_{13})_{jk}(\frac{m\pi}{a})\sum_{n=1}^{N_z} A_{kn}^{z} W_{mjn} + \\
&(c_{66})_{jk}(\frac{m\pi}{a}\sum_{n=1}^{N_y} A_{jn}^{y} V_{mnk} + \sum_{n=1}^{N_y} B_{jn}^{y} U_{mnk}) + \\
&(\frac{\partial c_{55}}{\partial z})_{jk}(\frac{m\pi}{a} W_{mjk} + \sum_{n=1}^{N_z} A_{kn}^{z} U_{mjn}) + \\
&(c_{55})_{jk}(\frac{m\pi}{a}\sum_{n=1}^{N_z} A_{kn}^{z} W_{mjn} + \sum_{n=1}^{N_z} B_{kn}^{z} U_{mjn}) = \\
&-\rho_{jk}\omega^2 U_{mjk}
\end{aligned} \tag{33}$$

in the y-direction:

$$\begin{aligned}
&(c_{66})_{jk}(-(\frac{m\pi}{a})^2 V_{mjk} + \\
&(\frac{-m\pi}{a})\sum_{n=1}^{N_y} A_{jn}^{y} U_{mnk}) + (c_{12})_{jk}((\frac{-m\pi}{a}) \\
&\sum_{n=1}^{N_y} A_{jn}^{y} U_{mnk}) + (c_{22})_{jk}\sum_{n=1}^{N_y} B_{jn}^{y} V_{mnk} + (c_{23})_{jk} \\
&(\sum_{n=1}^{N_y}\sum_{r=1}^{N_z} A_{kr}^{z} A_{jn}^{y} W_{mnr}) + (\frac{\partial c_{44}}{\partial z})_{jk}(\sum_{n=1}^{N_z} A_{kn}^{z} V_{mjn} + \\
&\sum_{n=1}^{N_y} A_{jn}^{y} W_{mnk}) + (c_{44})_{jk}(\sum_{n=1}^{N_z} B_{kn}^{z} V_{mjn} + \\
&\sum_{n=1}^{N_y}\sum_{r=1}^{N_z} A_{kr}^{z} A_{jn}^{y} W_{mnr}) = -\rho_{jk}\omega^2 V_{mjk}
\end{aligned} \tag{34}$$

and in the z-direction:

$$\begin{aligned}
&(c_{55})_{jk}(-(\frac{m\pi}{a})^2 W_{mjk} - \frac{m\pi}{a}\sum_{n=1}^{N_z} A_{kn}^{z} U_{mjn}) + \\
&(c_{44})_{jk}(\sum_{n=1}^{N_y}\sum_{r=1}^{N_z} A_{kr}^{z} A_{jn}^{y} V_{mnr} + \sum_{n=1}^{N_y} B_{jn}^{y} W_{mnk}) + \\
&(\frac{\partial c_{13}}{\partial z})_{jk}(-\frac{m\pi}{a} U_{mjk}) + (c_{13})_{jk}(-\frac{m\pi}{a} \\
&\sum_{n=1}^{N_z} A_{kn}^{z} U_{mjn}) + (\frac{\partial c_{23}}{\partial z})_{jk}\sum_{n=1}^{N_y} A_{jn}^{y} V_{mnk} + \\
&(c_{23})_{jk}\sum_{n=1}^{N_y}\sum_{r=1}^{N_z} A_{kr}^{z} A_{jn}^{y} V_{mnr} + (\frac{\partial c_{33}}{\partial z})_{jk} \\
&\sum_{n=1}^{N_z} A_{kn}^{z} W_{mjn} + (c_{33})_{jk}\sum_{n=1}^{N_z} B_{kn}^{z} W_{mjn} = -\rho_{jk}\omega^2 W_{mjk}
\end{aligned} \tag{35}$$

where A_{ij}^{y}, A_{ij}^{z}, and B_{ij}^{y}, B_{ij}^{z} are the first- and second-order DQ weighting coefficients in the *y*- and *z*-directions, respectively.

In a similar manner, boundary conditions can be discretized. To carry out an eigenvalue analysis, the domain and boundary nodal displacements should be separated. In vector forms, they are denoted as {d} and {b}, respectively. Based on this definition, the discretized form of the equations of motion and the related boundary conditions can be represented in the matrix form as equations of motion:

$$\left[\left[K_{db}\right]\left[K_{dd}\right]\right]\begin{Bmatrix}\{b\}\\ \{d\}\end{Bmatrix} - \omega^2\left[M\right]\{d\} = \{0\} \tag{36}$$

and as boundary conditions:

$$\left[K_{bd}\right]\{d\} + \left[K_{bb}\right]\{b\} = \{0\} \tag{37}$$

Eliminating the boundary degrees of freedom in (36) using (37), this equation becomes,

$$\left[K\right] - \omega^2\left[M\right]\{d\} = \{0\} \tag{1}$$

where $\left[K\right] = \left[K_{dd}\right] - \left[K_{db}\right]\left[K_{bb}\right]^{-1}\left[K_{bd}\right]$. The above eigenvalue system of equations can be solved to find the natural frequencies and mode shapes of the plates.

5. Numerical results and discussion

The study results were compared to those for 1-D conventional functionally graded rectangular plates, and presented formulations are given in the form of convergence studies with respect to N_z and N_y, which refer to the number of discrete points distributed along the thickness and width of the plate, respectively. The boundary conditions of the plate are specified by letters; for example, *S-C-S-F* denotes a plate with edges x=-*a/2* and *a/2* simply supported (*S*), edge y=-*b/2* clamped (*C*), and edge y=*b/2* free (*F*).

The properties of the plate were assumed to vary through the thickness of the plate with a desired variation of the volume fractions of the two materials in between the two surfaces. The modulus of elasticity E and mass density ρ were assumed to follow a simple power law distribution, and Poisson's ratio υ was assumed to be a constant, as follows:

$$E(z) = E_M + E_{CM}V_f, \upsilon(z) = \upsilon_0\rho(z) = \rho_M + \rho_{CM}V_f, \quad E_{CM} = E_C - E_M, \rho_{CM} = \rho_C - \rho_M, V_f = (0.5 + z/h)^p \tag{39}$$

where $-h/2 \le z \le h/2$ and p is the power law index that takes values greater than or equal to zero. Subscripts M and C refer to the metal and ceramic constituents that denote the material properties of the bottom and top surface of the plate, respectively. The mechanical properties are as follows:

Metal (Aluminum, Al):

$$E_M = 70*10^9\ N/m^2, \upsilon = 0.3, \rho_M = 2702\,kg/m^3$$

Ceramic (Alumina, Al_2O_3):

$$E_C = 380*10^9\ N/m^2, \upsilon = 0.3, \rho_C = 3800\,kg/m^3$$

In Table 5, the first seven non-dimensional natural frequency parameters of simply supported thick functionally graded plates are compared to those of Matsunaga [15] and Yas and Sobhani [14]. Ny and Nz are the number of discretised point in the y- and z-directions, and p is the exponent parameter in Table 5.

According to these data, excellent solution agreements can be observed between the present method and others. A numerical value of $N_z = N_y = 13$ was used, and the variation in CNT distribution through the plate was assumed to be as follows (Figure 4),

$$V_{cnt} = \begin{Bmatrix} 2*(\frac{2|z|}{h})*V^*_{CNT}, \text{FG}-\text{X(Type1)} \\ V^*_{CNT}, \text{UD(Type 2)} \\ (1+\frac{2z}{h})*V^*_{CNT}, \text{FG}-\Lambda\text{(Type 3)} \\ 2*(1-\frac{2|z|}{h})*V^*_{CNT}, \text{FG}-\Diamond\text{(Type 4)} \end{Bmatrix} \tag{40}$$

where V^*_{CNT} is the CNT volume fraction. It should be noted that, for both UD and functionally graded cases, the values of mass fractions of CNTs are the same.

After demonstrating the convergence and accuracy of the method, parametric studies for 3-D vibration analysis of functionally graded nanocomposite sandwich plates with various length-to-width ratios (a/b) and combinations of free, simply supported, and clamped boundary conditions at the edges were computed. A comprehensive study was also carried out to investigate the effect of CNT agglomeration on the vibrational response of sandwich structures.

Before analyzing the free vibration of functionally graded nanocomposite sandwich plates, the effects of agglomeration degree (μ and η) on the effective longitude Young's modulus and Poisson's ratio of UD-CNTRC plates were investigated (Figure 5.) Figure 5A represents the highest value for Young's moduli attained for the agglomeration state of $\mu = \eta$ (i.e., full dispersion), where the volume fraction of CNTs in the cluster and the matrix were equal. When μ was less than η ($\mu < \eta$), the effective Young's modulus increased as the value of μ increased, reaching a maximum value when the CNTs were uniformly dispersed in the composite (i.e., $\mu = \eta$ and for $\mu > \eta$); the effective stiffness decreased with the increase of μ. The effect of agglomeration degree on the Poisson's ratio for UD plates is plotted in Figure 5B. In contrast to Young's modulus behavior, with the increase of μ, Poisson's ratio decreased for $\mu < \eta$ and increased for $\mu > \eta$ due to the fact that the Poisson's ratio of the equivalent fiber described properties of the equivalent fiber section less than the Poisson's ratio of the matrix.

Using the relations presented in material properties of CNTRCs and problem description sections, variations in the effective material properties through the thickness of the FGS-CNTR plate for different agglomeration parameters were observed. For instance, by considering h_f/h=0.25, a=1, b=0, p=1, and V^*=20%, the variations in Young's moduli and Poisson's ratios for functionally graded sandwich plates with respect to the different agglomeration parameters μ and $\eta = 1$ are illustrated in Figures 6 and 7. As expected, at a constant z/h ratio, increases in parameter μ increased the effective Young's modulus and decreased the Poisson's ratio because $\mu < \eta = 1$.

The agglomeration parameters had significant effects on the material properties. Therefore, it is concluded that CNTs agglomeration plays an important role in vibrational characteristics of FGS-CNTR plates.

The free vibrational characteristics of FGS-CNTR plates was studied using an MT approach based on the equivalent fiber discussed in the properties of the equivalent fiber section and Table 1.

The non-dimensional natural frequency and Winkler and shearing layer elastic coefficients are as follows [67].

$$\Omega = \omega\frac{b^2}{\pi^2}\sqrt{\rho_m h/D_m}, D_m = E_m/12(1-\upsilon_m^2) \tag{41}$$

Table 5. Convergence behavior and accuracy of the first seven non-dimensional natural frequencies ($\varpi = \omega h\sqrt{\rho_C / E_C}$) of a simply supported functionally graded plate against the number of DQ grid points (b/h = 2)

P	N_z	N_y	ϖ_1	ϖ_2	ϖ_3	ϖ_4	ϖ_5	ϖ_6	ϖ_7
0	7	7	0.5569	0.9395	0.9735	1.3764	1.5072	1.6064	1.7384
		9	0.5570	0.9396	0.9741	1.3771	1.5083	1.6071	1.7401
		13	0.5570	0.9396	0.9740	1.3774	1.5088	1.6076	1.7407
	9	7	0.5573	0.9398	0.9735	1.3771	1.5087	1.6074	1.7403
		9	0.5572	0.9400	0.9742	1.3777	1.5090	1.6079	1.7406
		13	0.5572	0.9400	0.9741	1.3778	1.5096	1.6086	1.7405
	13	7	0.5571	0.9401	0.9735	1.3779	1.5094	1.6083	1.7411
		9	0.5572	0.9400	0.9742	1.3777	1.5090	1.6078	1.7405
		13	0.5572	0.9400	0.9742	1.3777	1.5090	1.6078	1.7406
		[15]	0.5572	0.9400	0.9742	1.3777	1.5090	1.6078	1.7406
		[14]	0.557243	0.940041	-	-	1.508987	-	1.740602
0.5	7	7	0.4829	0.8222	0.8700	1.2250	1.3332	1.4364	1.5401
		9	0.4828	0.8229	0.8707	1.2258	1.3337	1.4367	1.5429
		13	0.4830	0.8224	0.8706	1.2254	1.3338	1.4370	1.5424
	9	7	0.4833	0.8225	0.8701	1.2251	1.3335	1.4365	1.5402
		9	0.4835	0.8240	0.8708	1.2257	1.3340	1.4370	1.5431
		13	0.4836	0.8233	0.8707	1.2258	1.3340	1.4369	1.5426
	13	7	0.4836	0.8227	0.8701	1.2251	1.3334	1.4366	1.5402
		9	0.4835	0.8231	0.8708	1.2259	1.3338	1.4370	1.5431
		13	0.4835	0.8233	0.8709	1.2259	1.3339	1.4370	1.5425
		[15]	0.4835	0.8233	0.8709	1.2259	1.3339	1.4370	1.5425
		[14]	0.482849	0.822358	-	-	1.332605	-	1.541085
1	7	7	0.4367	0.7476	0.7997	1.1158	1.2154	1.3085	1.4059
		9	0.4374	0.7477	0.8001	1.1165	1.2159	1.3090	1.4075
		13	0.4373	0.7478	0.8005	1.1163	1.2162	1.3088	1.4077
	9	7	0.4368	0.7477	0.7998	1.1159	1.2157	1.3088	1.4068
		9	0.4374	0.7477	0.8003	1.1165	1.2161	1.3090	1.4076
		13	0.4374	0.7478	0.8006	1.1165	1.2162	1.3090	1.4078
	13	7	0.4368	0.7477	0.7999	1.1159	1.2158	1.3088	1.4070
		9	0.4375	0.7478	0.8003	1.1165	1.2162	1.3091	1.4076
		13	0.4375	0.7478	0.8005	1.1165	1.2163	1.3091	1.4077
		[15]	0.4375	0.7477	0.8005	1.1166	1.2163	1.3091	1.4078
		[14]	0.437396	0.747514	-	-	1.216035	-	1.407459
4	7	7	0.3565	0.5988	0.6249	0.8724	0.9589	1.0000	1.1029
		9	0.3577	0.5995	0.6355	0.8729	0.9589	1.0007	1.1038
		13	0.3577	0.5996	0.6349	0.8728	0.9589	1.0003	1.1030
	9	7	0.3569	0.5989	0.6250	0.8726	0.9589	1.0001	1.1032
		9	0.3579	0.5997	0.6357	0.8731	0.9589	1.0008	1.1040
		13	0.3578	0.5997	0.6351	0.8730	0.9589	1.0005	1.1032
	13	7	0.3571	0.5991	0.6252	0.8727	0.9589	1.0001	1.1033
		9	0.3579	0.5997	0.6357	0.8731	0.9589	1.0008	1.1040
		13	0.3579	0.5997	0.6352	0.8731	0.9589	1.0008	1.1040
		[15]	0.3579	0.5997	0.6352	0.8731	0.9591	1.0008	1.1040
		[14]	0.357758	0.599494	-	-	0.958764	-	1.103674
10	7	7	0.3306	0.5454	0.5657	0.7866	0.8588	0.9043	0.9838
		9	0.3311	0.5460	0.5662	0.7890	0.8588	0.9047	0.9841
		13	0.3310	0.5459	0.5661	0.7881	0.8588	0.9050	0.9846
	9	7	0.3308	0.5455	0.5659	0.7870	0.8588	0.9044	0.9840
		9	0.3313	0.5461	0.5664	0.7892	0.8588	0.9048	0.9842
		13	0.3312	0.5460	0.5663	0.7883	0.8588	0.9051	0.9846
	13	7	0.3309	0.5455	0.5660	0.7871	0.8588	0.9045	0.9840
		9	0.3313	0.5461	0.5664	0.7892	0.8588	0.9049	0.9844
		13	0.3313	0.5461	0.5664	0.7884	0.8588	0.9051	0.9847
		[15]	0.3313	0.5460	0.5664	0.7885	0.8588	0.9050	0.9847
		[14]	0.331146	0.545833	-	-	0.858445	-	0.984365

To compare vibrational responses from a single-layer functionally graded plate and a functionally graded laminated plate, a special case was considered: h_f/h=0.3, a=1, b=0, p=1, and V^*=20%. The variations in CNT volume fractions through the thickness of the FGS-CNTR plate can be found in Figure 8.

The effect of agglomeration on vibrational response of functionally graded plates for different boundary conditions are depicted in Figure 9. The lowest magnitude frequency parameter was obtained using a type 4 functionally graded plate, followed by types 3, 2, 1, and the functionally graded sandwich plate. For many η, for instance $\eta = 1$, and for small amounts of μ, the functionally graded sandwich plates had lower frequency amounts than functionally graded type 1 plates.

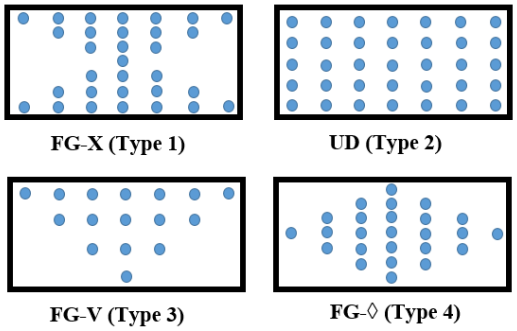

Figure 4. Schematic configuration of a CNT-reinforced composite plate with four types of CNT distribution

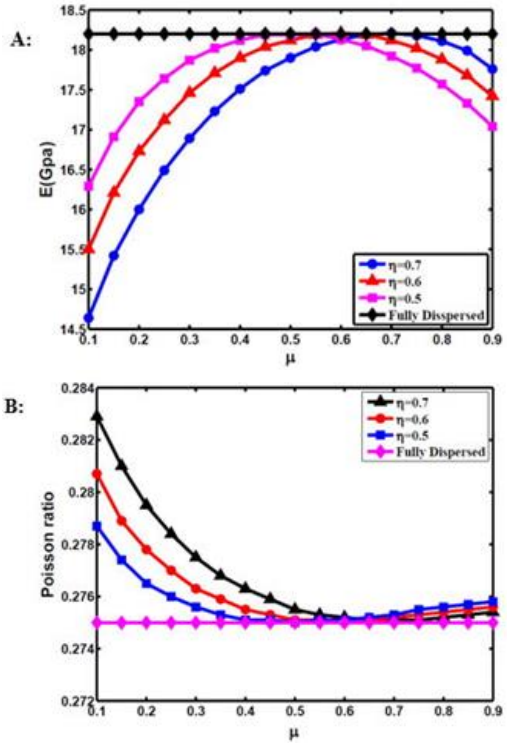

Figure 5. Influence of CNT agglomeration parameters. μ .and η on the (A) effective Young's modulus and (B) Poisson's ratio of the UD nanocomposite plate

According to Figure 9, for all types of CNT distribution, with the increase of μ, the frequency parameters increased. Discrepancies between frequencies for the plates with type 3 and type 2 material distribution of CNTs remained almost unaltered with increases in μ.

Figure 10 shows that for lower amounts of η the frequency response of plates with different types of material distribution changed. This figure reveal that with increases in μ, the natural frequency increased, but when μ was more than 0.5, the frequency parameters tended to decrease.

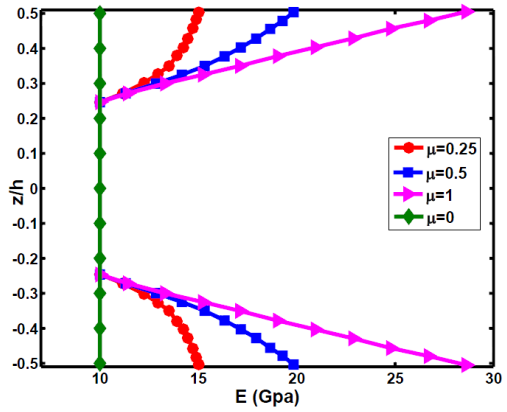

Figure 6. The variation in Young's moduli along the thickness of the FGS-CNTR plate with the agglomeration effect

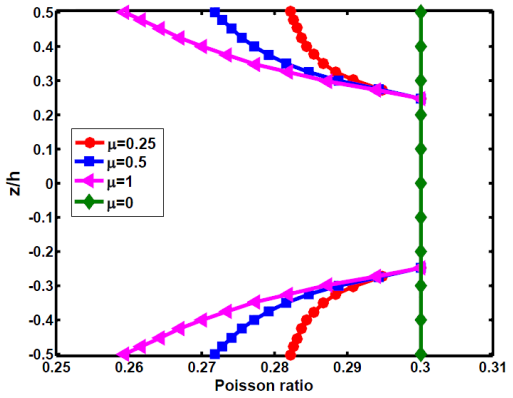

Figure 7. The variation of Poisson's ratio along the thickness of the FGS-CNTR plate with the agglomeration effect

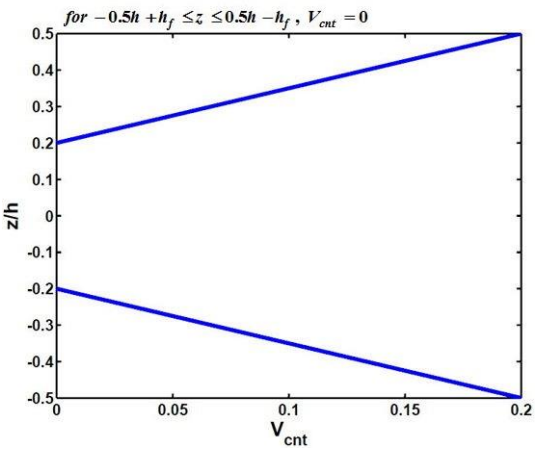

Figure 8. Variations in CNT volume fractions through the thickness of FGS-CNTR plates

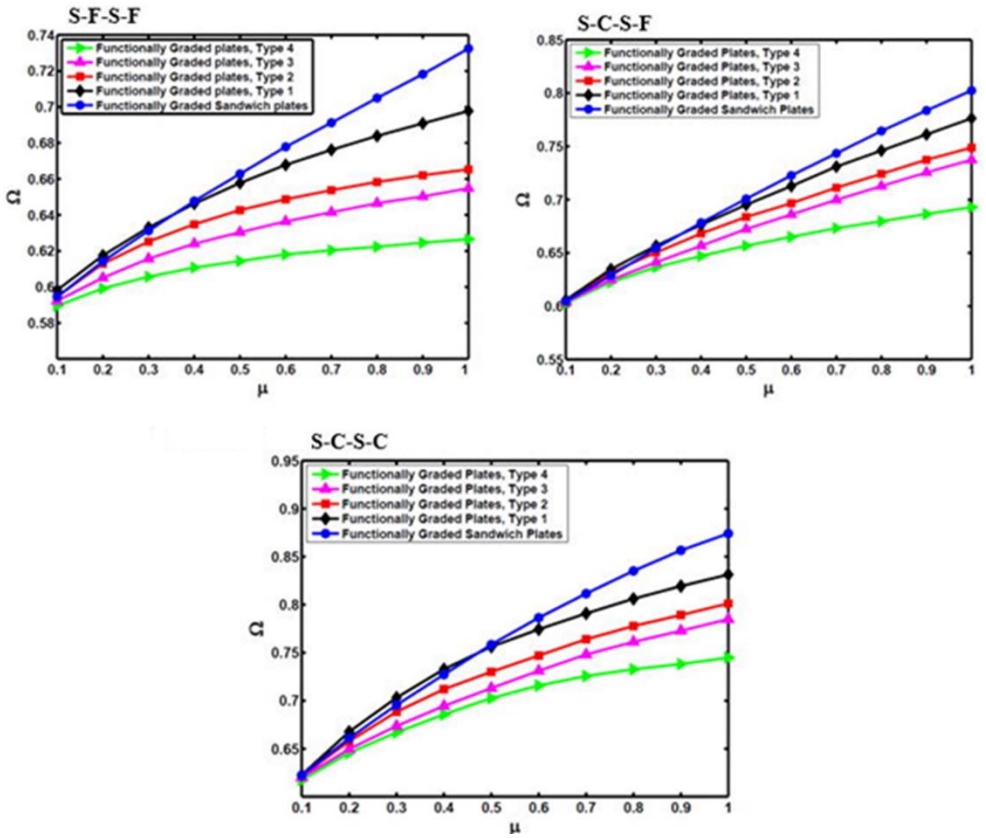

Figure 9. The variation of frequency parameters versus agglomeration parameters for different types of CNTRC plates and boundary conditions ($\eta = 1$, a/b=1, b/h=2)

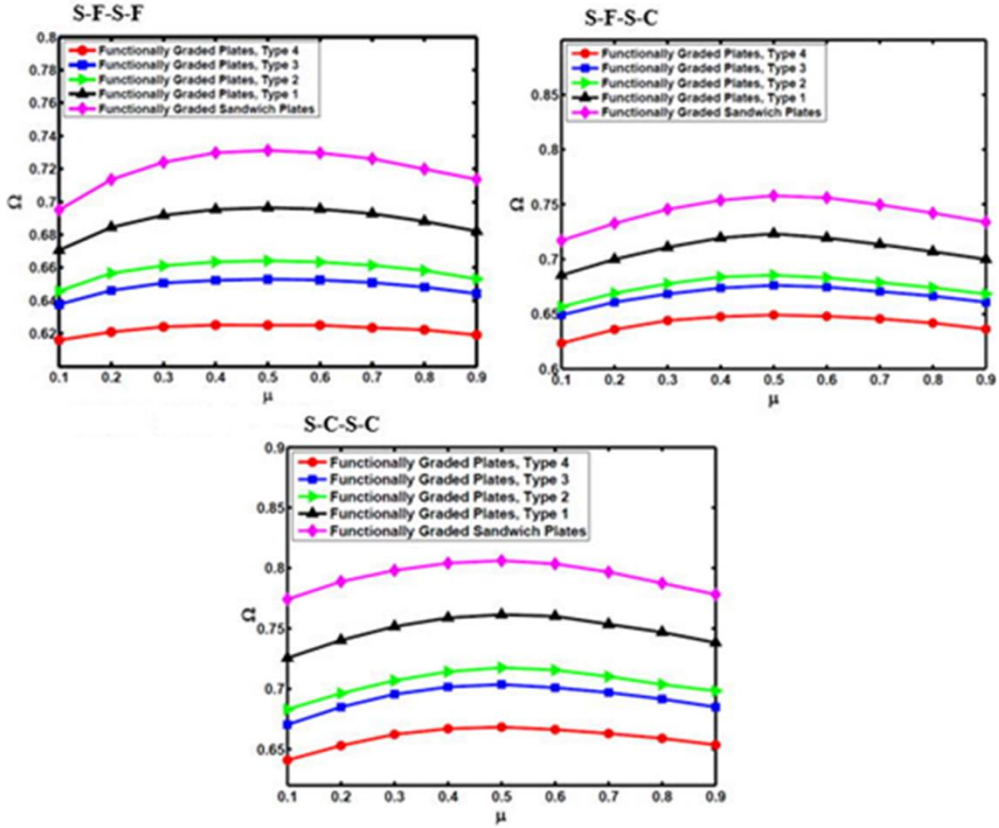

Figure 10. The variation of frequency parameters versus agglomeration parameters for different types of CNTRC plates and boundary conditions (η=0.5, a/b=1, b/h=2)

The effect of material distributions and total volume percentage of CNTs (V_{cnt}^{total}) on the vibrational response of sandwich plates were investigated. It should be noted that various material profiles can be obtained by considering different amounts for parameters *a*, *c*, and *p.*

The influence of index *p* and parameter *a* on the fundamental frequency parameters of FGS-CNTR plates is shown in Figure 11 for S-F-S-F, S-F-S-C, and S-C-S-C boundary conditions. The figure shows the fundamental frequency parameters of the FGS-CNTR plate versus the power-law index *p* for various values of the parameter *a*, when *b* = 0.3 and *c* = 3. Increases in parameter *p* caused the frequency parameter of sandwich plates to also increase. For small amounts of *a*, the frequency parameter steadily increased, but for greater amounts of this parameter, the increase in frequency parameters was more significant. To have a better understanding, the material distribution profiles in Figure 11 are provided in Figures 12, 13, and 14 for different amounts of parameters a and p.

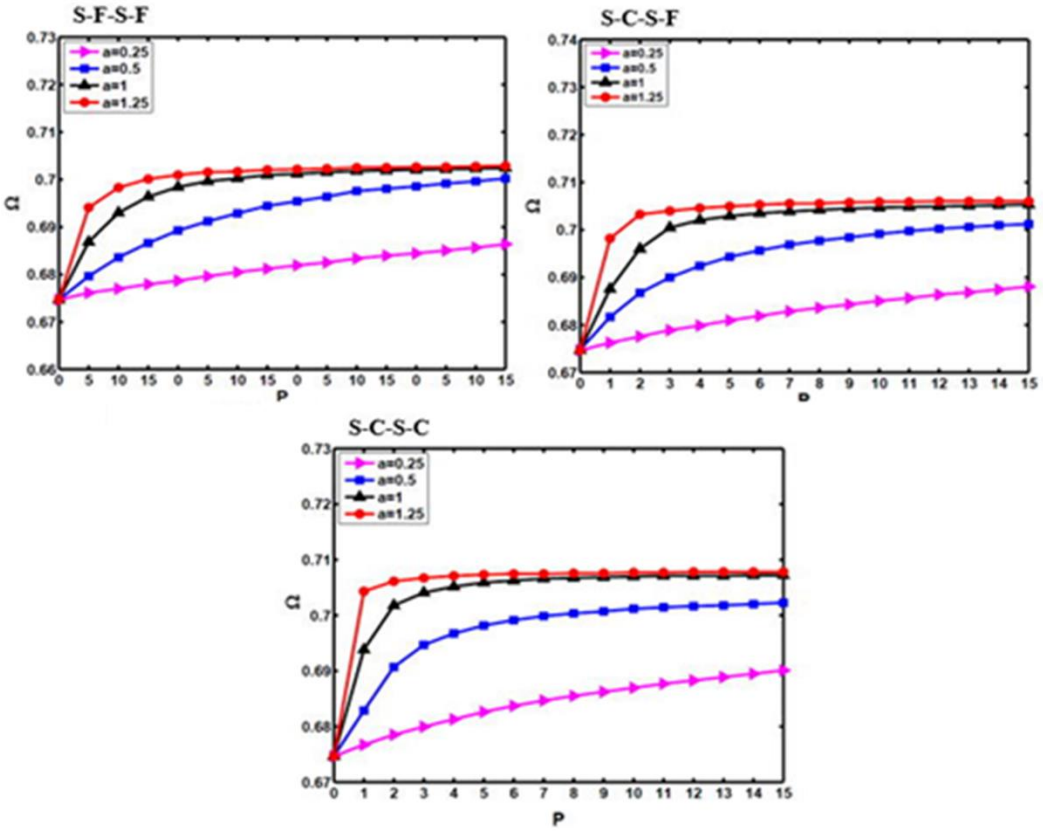

Figure 11. Variation of the fundamental frequency parameter of CNTR plates for different types of boundary conditions versus the power-law exponent p (*a*/*b* = 1, b/h = 2)

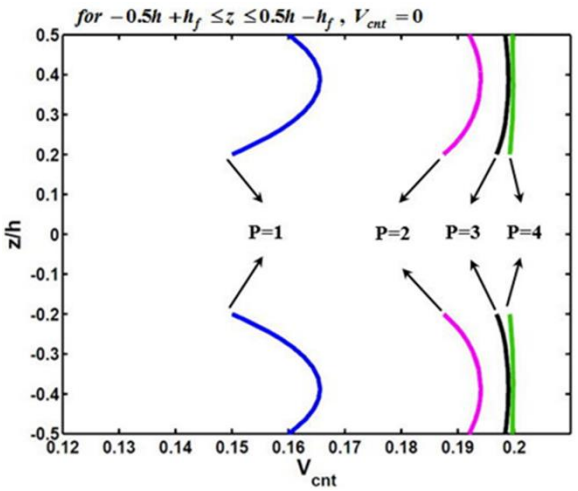

Figure 12. The material distribution profiles for thickness of sandwich plates (*a* = 0.25, *b* = 0.2, *c* = 2).

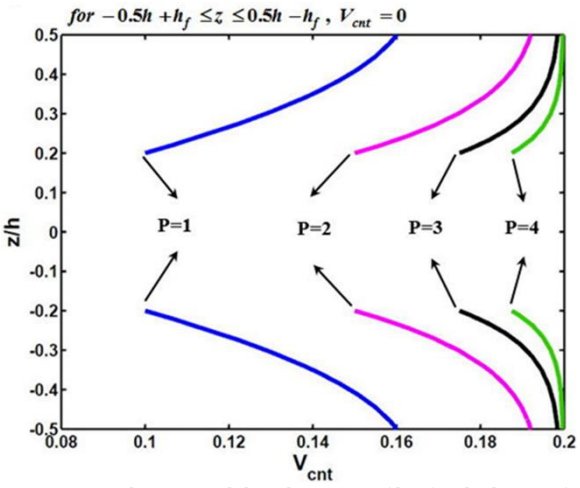

Figure 13. The material distribution profiles for thickness of sandwich plates (*a* = 0.5, *b* = 0.2, *c* = 2).

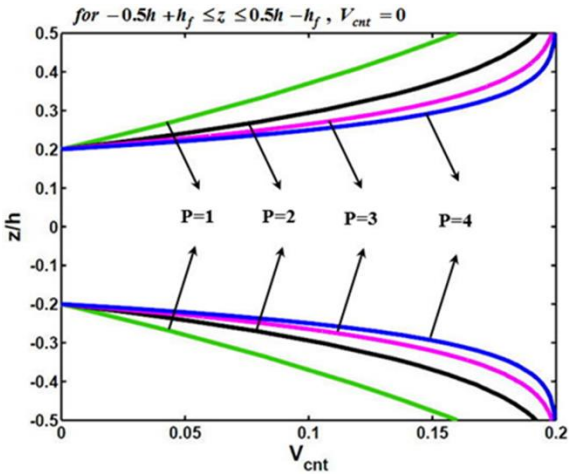

Figure 14. The material distribution profiles for thickness of sandwich plates (a = 1, b = 0.2, c = 2).

The influence of parameter c on the free vibration of sandwich plates with FG-CNTR face sheets was investigated and is presented in Figure 15. Parameter c varied from 2 to 12, and as it increased, the fundamental frequency increased due to the CNT volume fraction and, therefore, the frequency parameters also increasing. This behavior was observed for two types of boundary conditions that are not shown here for brevity's sake. The material distribution profiles for the results in Figure 15 are provided in Figures 16, 17, 18, and 19.

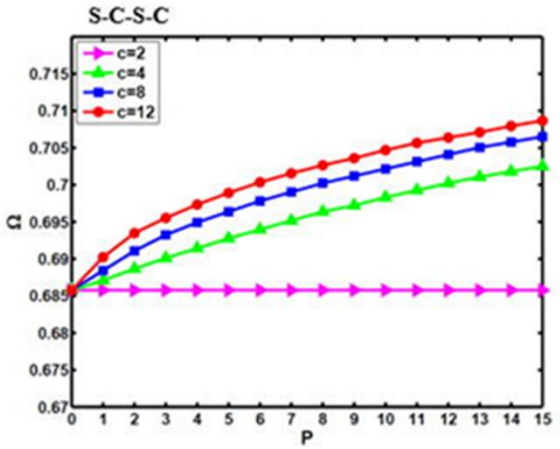

Figure 15. Variation in the fundamental frequency parameter of FGS-CNTR plates versus the power-law exponent p (a/b = 1, b/h = 2)

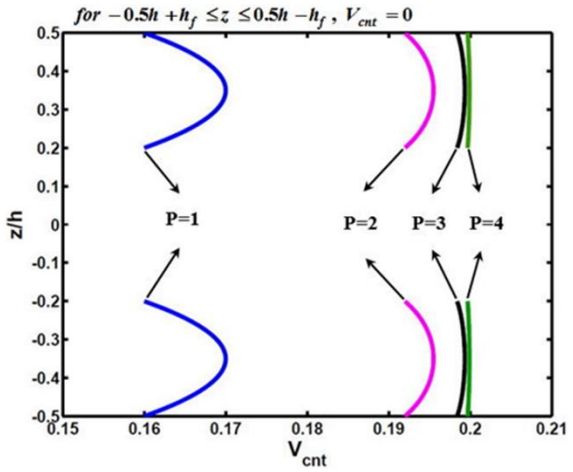

Figure 16. The material distribution profiles for thickness of sandwich plates (a = 0.2, b = 0.2, c = 2).

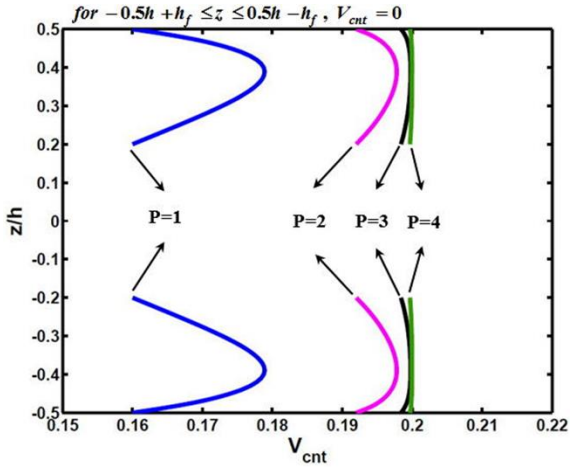

Figure 17. The material distribution profiles for thickness of sandwich plates (a = 0.2, b = 0.2, c = 4).

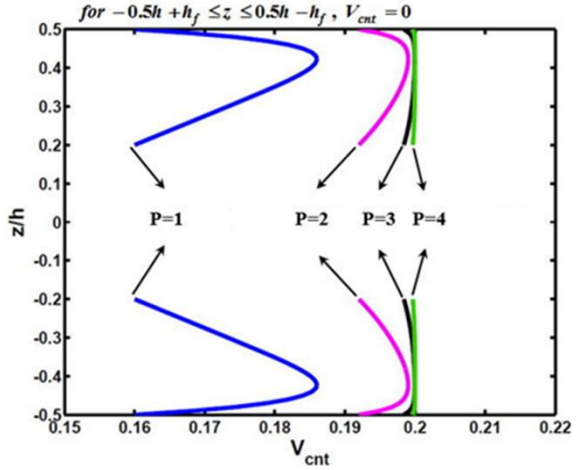

Figure 18. The material distribution profiles for thickness of sandwich plates (a = 0.2, b = 0.2, c = 8).

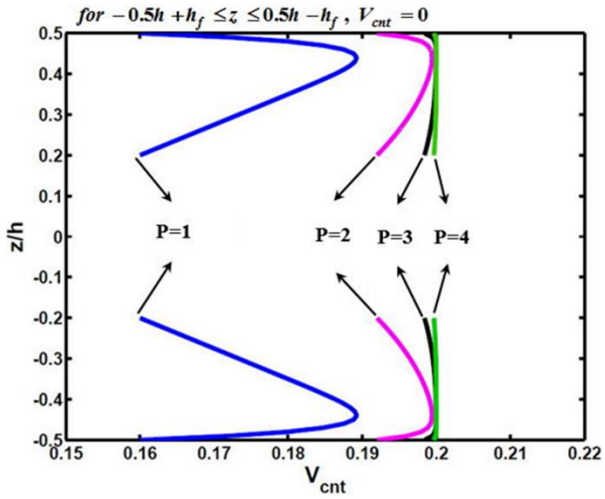

Figure 19. The material distribution profiles for thickness of sandwich plates (a = 0.2, b = 0.2, c = 12).

6. Conclusion

In this research, the 2-D generalized DQM was employed to obtain a highly accurate semi-analytical solution for free vibration of functionally graded nanocomposite sandwich plates under various boundary conditions. The study was carried out based on the 3-D, linear, and small strain elasticity theories. The MT approach was implemented to estimate the effective material properties of the nanocomposite sandwich plates. The agglomeration effect of single-walled CNTs was and was shown to significantly affect the natural frequencies of structures, as well as mechanical properties and, therefore, free vibrations of FGS-CNTR plates. It was found that, except in some states, functionally graded structures improve the vibrational characteristics of CNTRCs. The effects of different boundary conditions, various geometric parameters, and different material profiles along the thickness of sandwich rectangular plates were also investigated.

References

[1] Koizumi M. The concept of FGM, ceramic transactions. *Funct Gradient Mater* 1993; 34: 3-10.

[2] Malekzadeh P, Golbahar Haghighi MR, Atashi MM. Free vibration analysis of elastically supported functionally graded annular plates subjected to thermal environment. *Meccanica* 2011; 46(5): 893-913.

[3] Hosseini-Hashemi S, Es'haghi M, Karimi M. Closed-form vibration analysis of thick annular functionally graded plates with integrated piezoelectric layers. *Int J Mech Sci* 2010; 52(3): 410-428.

[4] Nie GJ, Zhong Z. Vibration analysis of functionally graded annular sectorial plates with simply supported radial edges. *Compos Struct* 2008; 84(2): 167-176.

[5] Yas MH, Tahouneh V. 3-D free vibration analysis of thick functionally graded annular plates on Pasternak elastic foundation via differential quadrature method (DQM). *Acta Mech* 2012; 223(1): 43-62.

[6] Tahouneh V, Yas MH. 3-D free vibration analysis of thick functionally graded annular sector plates on Pasternak elastic foundation via 2-D differential quadrature method. *Acta Mech* 2012; 223(9): 1879-1897.

[7] Tahouneh V, Yas M.H. Semi-analytical solution for three-dimensional vibration analysis of thick multidirectional functionally graded annular sector plates under various boundary conditions. *J Eng Mech* 2013; 140(1): 31-46.

[8] Tahouneh V. Free vibration analysis of bidirectional functionally graded annular plates resting on elastic foundations using differential quadrature method. *Structural Engineering and Mechanics, An Int'l Journal* 2014a; 52(4): 663-686.

[9] Tahouneh V. Free vibration analysis of thick CGFR annular sector plates resting on elastic foundations. *Structural Engineering and Mechanics, An Int'l Journal* 2014b; 50(6): 773-796.

[10] Tahouneh V, Yas MH, Tourang H, Kabirian M. Semi-analytical solution for three-dimensional vibration of thick continuous grading fiber reinforced (CGFR) annular plates on Pasternak elastic foundations with arbitrary boundary conditions on their circular edges. *Meccanica* 2013; 48(6): 1313-1336.

[11] Arefi M. Elastic solution of a curved beam made of functionally graded materials with different cross sections. *Steel and Composite Structures An Int'l Journal* 2015; 18(3): 659-672.

[12] Bennai R, Ait Atmane H, Tounsi A. A new higher-order shear and normal deformation theory for functionally graded sandwich beams. *Steel and Composite Structures, An Int'l Journal* 2015; 19(3): 521-546.

[13] Tahouneh V. Using an equivalent continuum model for 3D dynamic analysis of nanocomposite plates. *Steel and Composite Structures, An Int'l Journal* 2016; 20(3): 623-649, 2016.

[14] Yas MH, Sobhani Aragh B. Free vibration analysis of continuous grading fiber reinforced plates on elastic foundation. *Int J Eng Sci* 2010; 48(12): 1881-1895.

[15] Matsunaga H. Free vibration and stability of functionally graded plates according to a 2D higher-order deformation theory. *J Compos Struct* 2008; 82(4): 499-512.

[16] Hosseini-Hashemi S, Rokni Damavandi T, Akhavan H. Vibration analysis of radially FGM sectorial plates of variable thickness on elastic foundations. *Compos Struct* 2010; 92(7): 1734-1743.

[17] Salvetat D, Rubio A. Mechanical properties of carbon nanotubes: a fiber digest for beginners. *Carbon* 2002; 40(10): 1729-1734.
[18] Wernik JM, Meguid SA. Multiscale modeling of the nonlinear response of nano-reinforced polymers. *Acta Mech* 2011; 217(1): 1-16.
[19] Thostenson ET, Ren ZF, Chou TW. Advances in the Science and Technology of Carbon Nanotubes and their Composites: A Review. *Compos Sci Technol* 2001; 61(13): 1899-1912.
[20] Moniruzzaman M, Winey KI. Polymer nanocomposites containing carbon nanotubes. *Macromolecules* 2006; 39(16): 5194-5205.
[21] Valter B, Ram MK, Nicolini C. Synthesis of multiwalled carbon nanotubes and poly (o-anisidine) nanocomposite material: fabrication and characterization its langmuir-schaefer films. *Langmuir* 2002; 18(5): 1535-1541.
[22] Qian D, Dickey EC, Andrews R, Rantell T. Load transfer and deformation mechanisms in carbon nanotube-polystyrene composites. *Appl Phys Lett* 2000; 76(20): 2868-2870.
[23] Yokozeki T, Y Iwahori Y, Ishiwata S. Matrix cracking behaviors in carbon fiber/epoxy laminates filled with cup-stacked carbon nanotubes (CSCNTs). *Compos Part A* 2007; 38(3): 917-924.
[24] Shokrieh MM, Rafiee R. Prediction of mechanical properties of an embedded carbon nanotube in polymer matrix based on developing an equivalent long fiber. *Mech Res Commun* 2010; 37(2): 235-240.
[25] Seidel GD, Lagoudas DC. Micromechanical analysis of the effective elastic properties of carbon nanotube reinforced composites. *Mech Mater* 2006; 38(8-10): 884-907.
[26] Shen HS. Nonlinear bending of functionally graded carbon nanotube-reinforced composite plates in thermal environments. *Compos. Struct* 2009; 91(1): 9-19.
[27] Shen HS, Zhu ZH. Buckling and postbuckling behavior of functionally graded nanotube-reinforced composite plates in thermal environments. *Comput Mater Continua* 2010; 18(2): 155-182.
[28] Shen HS, Zhang CL. Thermal buckling and postbuckling behavior of functionally graded carbon nanotube-reinforced composite plates. *Mater Des* 2010; 31(7): 3403-3411.
[29] Ke LL, Yang J, Kitipornchai S. Nonlinear free vibration of functionally graded carbon nanotube-reinforced composite beams. *Compos Struct* 2010; 92(3): 676-683.
[30] Marin M, Lupu M. On harmonic vibrations in thermoelasticity of micropolar bodies. *J Vib Control* 1998; 4(5): 507-518.
[31] Marin M. A domain of influence theorem for microstretch elastic materials, *Nonlinear Anal. Real World Appl* 2010; 11(5): 3446-3452.
[32] Sharma K, Marin M. Effect of distinct conductive and thermodynamic temperatures on the reflection of plane waves in micropolar elastic halfspace. *UPB Sci Bull Series A-Appl Math Phys* 2013; 75(2): 121-132.
[33] Anderson TA. A 3-D elasticity solution for a sandwich composite with functionally graded core subjected to transverse loading by a rigid sphere. *Compos Struct* 2003; 60(3): 265-274.
[34] Kashtalyan M, Menshykova M. Three-dimensional elasticity solution for sandwich panels with a functionally graded core. *Compos Struct* 2009; 87(1): 36-43.
[35] Li Q, Iu V, Kou K. Three-dimensional vibration analysis of functionally graded material sandwich plates. *J Sound Vib* 2008; 311(1-2): 498-515.
[36] Kamarian S, Yas MH, Pourasghar A. Free vibration analysis of three-parameter functionally graded material sandwich plates resting on Pasternak foundations. *J Sandw Struct Mater* 2013; 15(3): 292-308.
[37] Wang ZX, Shen, HS. Nonlinear vibration and bending of sandwich plates with nanotube-reinforced composite face sheets. *Compos Part B* 2011; 43(2): 411-421.
[38] Tahouneh V, Naei MH. Free vibration and vibrational displacements analysis of thick elastically supported laminated curved panels with power-law distribution functionally graded layers and finite length via 2D GDQ method. *J Sandw Struct Mater* 2016; 18(3): 263-293.
[39] Moradi-Dastjerdi R. Wave propagation in functionally graded composite cylinders reinforced by aggregated carbon nanotube. *Struct Eng Mech* 2016; 57: 441-456.
[40] Moradi-Dastjerdi R, Momeni-Khabisi H. Vibrational behavior of sandwich plates with functionally graded wavy carbon nanotube-reinforced face sheets resting on Pasternak elastic foundation. *J Vib Conrol* 2017; DOI: 10.1177/1077546316686227.
[41] Moradi-Dastjerdi R, Momeni-Khabisi H. Dynamic analysis of functionally graded nanocomposite plates reinforced by wavy carbon nanotube. *Steel and Composite Structures* 2016; 22: 277-299.
[42] Moradi-Dastjerdi R, Malek-Mohammadi H. Biaxial buckling analysis of functionally graded nano composite sandwich plates reinforced by aggregated carbon nanotube using improved high-order theory. *J Sandw Struct Mater* 2016; 1099636216643425.

[43] Moradi-Dastjerdi R, Payganeh G, Malek-Mohammadi H. Free vibration analyses of functionally graded CNT reinforced nanocomposite sandwich plates resting on elastic foundation. *Journal of Solid Mechanics* 2015; 7: 158-172.

[44] Moradi-Dastjerdi R, Payganeh G, Tajdari M. The Effects of Carbon Nanotube Orientation and Aggregation on Static Behavior of Functionally Graded Nanocomposite Cylinders. *Journal of Solid Mechanics* 2017; 9: 198-212.

[45] Moradi-dastjerdi R, Malek-Mohammadi H. Free vibration and buckling analyses of functionally graded nanocomposite plates reinforced by carbon nanotube. *Mechanics of Advanced Composite Structures* 2017; 4: 59-73.

[46] Bouchafa A, Bouiadjra MB, Houari MSA, Tounsi A. Thermal stresses and deflections of functionally graded sandwich plates using a new refined hyperbolic shear deformation theory. *Steel and Composite Structures, An Int'l Journal* 2015; 18(6): 1493-1515.

[47] Shaffer MSP, Windle AH. Fabrication and Characterization of Carbon Nanotube/Poly (vinyl alcohol) *Composites. Adv Mater* (Weinheim Ger) 1999; 11(11): 937-941.

[48] Vigolo B, Penicaud AP, Couloun C, Sauder S, Pailler R, Journet C, Bernier P, Poulin P. Macroscopic fibers and ribbons of oriented carbon nanotubes. *Science* 2000; 290(5495): 1331-1334.

[49] Shi DL, Feng XQ, Huang YY, Hwang KC, Gao H. The effect of nanotube waviness and agglomeration on the elastic property of carbon nanotube reinforced composites. *J Eng Mater Technol* 2004; 126(3): 250-257.

[50] Wuite J, Adali S. Deflection and stress behaviour of nanocomposite reinforced beams using a multiscale analysis. *Compos Struct* 2005; 71(3-4): 388-396.

[51] Stephan C, Nguyen TP, Chapelle ML, Lefrant S. Characterization of single-walled carbon nanotubes-PMMA composite. *Synth Met* 2000; 108(2): 139-149.

[52] Kamarian S, Salim M, Dimitri R, Tornabene F. Free Vibration Analysis of Conical Shells Reinforced with Agglomerated Carbon Nanotubes. *Int J Mech Sci* 2016; 108(1): 157-165.

[53] Kamarian S, Shakeri M, Yas MH, Bodaghi M, Pourasghar A. Free vibration analysis of functionally graded nanocomposite sandwich beams resting on Pasternak foundation by considering the agglomeration effect of CNTs. *J Sandw Struct Mater*2015; DOI: 10.1177/1099636215590280.

[54] Heshmati M, Yas MH. Free vibration analysis of functionally graded CNT-reinforced nanocomposite beam using Eshelby-Mori-Tanaka approach. *J Mech Sci Technol* 2013; 27(11): 3403-3408.

[55] Tornabene F, Fantuzzi N, Bacciocchi M, Viola E. Effect of Agglomeration on the Natural Frequencies of Functionally Graded Carbon Nanotube-Reinforced Laminated Composite Doubly-Curved Shells. *Composites Part B* 2016; 89(1): 187-218.

[56] Moradi-Dastjerdi R, Pourasghar A, Foroutan M. The effects of carbon nanotube orientation and aggregation on vibrational behavior of functionally graded nanocomposite cylinders by a mesh-free method. *Acta Mech* 2013; 224(11): 2817-2832.

[57] Tornabene F, Fantuzzi N, Bacciocchi M. Linear static response of nanocomposite plates and shells reinforced by agglomerated carbon nanotubes. *Composite part B* 2017; 115: 449-476.

[58] Fantuzzi N, Tornabene F, Bacciocchi M, Dimitri R. Free vibration analysis of arbitrarily shaped functionally graded carbon nanotube-reinforced plates. *Composite part B* 2017; 115: 384-408.

[59] Pouresmaeeli S, Fazelzadeh SA, Ghavanloo E. Buckling Analysis of Spherical Composite Panels Reinforced by Carbon Nanotube. *Mechanics of Advanced Composite Structures* 2015; 2(2): 135-144.

[60] Tahouneh V, Eskandari-Jam J. A semi-analytical solution for 3-D dynamic analysis of thick continuously graded carbon nanotube-reinforced annular plates resting on a Two-parameter elastic foundation. *Mechanics of Advanced Composite Structures* 2014; 1(2): 113-130.

[61] Odegard GM, Gates TS, Wise KE, Park C, Siochi EJ. Constitutive modelling of nanotube reinforced polymer composites. *Compos Sci Technol* 2003; 63(11): 1671-1687.

[62] Tsai SW, Hoa CV, Gay D. **Composite materials, design and applications**. Boca Raton: CRC Press, 2003.

[63] Tornabene F, Viola E. Free vibration analysis of four-parameter functionally graded parabolic panels and shells of revolution. *Eur J Mech A/Solid* 2009; 28(5): 991-1013.

[64] Reddy JN. An **Introduction to Continuum Mechanics**, Second Edition, Cambridge University Press, 2013.

[65] Shu C. **Differential quadrature and its application in engineering**. Springer Science & Business Media, 2000.

[66] Shu C, Richards BE. Application of generalized differential quadrature to solve two dimensional incompressible Navier-Stokes equations. *Int J Numer Methods Fluid* 1992; 15(7): 791-798.

[67] Tahouneh V, Naei MH. A novel 2-D six-parameter power-law distribution for three-dimensional dynamic analysis of thick multi-directional functionally graded rectangular plates resting on a two-parameter elastic foundation. *Meccanica* 2014; 49(1): 91-109.